10th International Workshop on Ship and Marine Hydrodynamics
Keelung, Taiwan, November 5-8, 2017

A Fully Coupled Simulation Method for Floating Offshore Wind Turbine Dynamics Using a Boundary Element Method in Time Domain

Stefan Netzband*, Christian W. Schulz, Moustafa Abdel-Maksoud
Hamburg University of Technology, Am Schwarzenberg-Campus 4, 21073 Hamburg, Germany

*Corresponding author, stefan.netzband@tu-harburg.de

ABSTRACT

Predicting the dynamic behaviour of a floating offshore wind turbine (FOWT) is extremely demanding for common simulation methods because the floating structure motion is strongly influenced by complex aero- and hydrodynamics, inertia, and mooring loads. In order to provide a framework that can capture these effects in time domain, the in-house first-order panel method *pan*MARE is further developed. Both the aerodynamics of the rotor and the hydrodynamics of the platform are simulated with *pan*MARE and an integrated six-degrees-of-freedom solver is applied to predict the motions over time.

The hydrodynamic loads on the platform are simulated using the current floating condition including the instantaneous wetted surface while considering added mass effects and Froude-Krylov forces. Drag effects are considered using body-dependent coefficients.

Regarding the aerodynamics, the potential theory based method is capable of modelling the three-dimensional flow field of a wind turbine and therefore can consider the dynamics of rotor motions and the blade-wake interaction. Especially in the case of a pitching platform the effect of blade-wake interaction can have a significant impact on the aerodynamic loads. This effect can be captured by *pan*MARE. Aerodynamic drag forces due to friction are incorporated using a Reynolds-number-dependent friction model.

In this paper, the motion of the DeepCWind semisubmersible platform is compared with the results of the published code-to-code comparison OC4 Phase II and therefore evidence is provided for the validity of our method. The comparison is carried out for several load cases. The results show that *pan*MARE is capable of providing accurate simulations for decay test cases as well as capturing the influence of wind-wave and wind-current misalignments in time domain while modelling the wind turbine wake in a realistic manner. In addition, an analysis of the FOWT in yawed conditions is included in order to investigate the self-aligning capabilities and effects due to yawing in detail.

1 INTRODUCTION

In the last decade, offshore wind turbines (OWTs) proved to be a technically feasible and economically promising alternative to conventional power plants. The small ecological footprint of this technology offers the opportunity to decrease environmental damage caused by human energy production. Unfortunately, shallow water zones are rare in many regions of the world and therefore ground fixed structures are not economically viable there. In order to solve the issue of limited shallow water zones, floating offshore wind turbines (FOWTs) have increasingly attracted the attention of researchers and the industry.

As the technical feasibility has been demonstrated by different full-scale prototypes (e.g. Hywind or WindFloat), the next challenge is to reduce production and installation costs by further developing and optimising present and new FOWT designs. Precise load and motion prediction is one of the key aspects when reducing material usage and improving the impact stability of the designs. Ultimate and fatigue limit states need to be modelled accurately in order to assure a safe and reliable operation, on the one hand, and avoid oversizing the floating structure, on the other hand. Especially ultimate limit states – often occurring in extreme waves – require completely resolved flow fields and platform motions in time and space because the unsteady platform motion needs to be predicted in a realistic manner in every time instant to determine the resulting loads. Most simulation methods make use of engineering models for both aerodynamic and hydrodynamic

load prediction without modelling the unsteady flow regimes near the FOWT. To overcome these limitations, we introduce a new simulation approach which considers the three-dimensional aerodynamic and hydrodynamic flow fields in time domain using a potential flow theory based method for both flow fields.

Frequently used blade element momentum theory (BEMT) methods capture the wake's influence on the rotor blades via analytical induction factors resulting from the momentum balance and lift and drag coefficients of the blade sections. The vortex structure of the wake is not explicitly modelled in these methods. This approach is well suited for ground fixed wind turbines because the wake's influence on the rotor can be assumed constant at a certain wind speed with sufficient accuracy. Therefore, BEMT based methods have proven to deliver realistic load predictions for onshore wind turbines [1, 2] and have evolved to the state-of-the-art for industrial applications. As the rotor of an FOWT can move relative to its own wake, the wake's influence on the rotor becomes highly unsteady which cannot be captured by typical formulations of BEMT methods [3]. Our in-house panel method *pan*MARE (**pan**el Code for **M**aritime **A**pplications and **RE**search) considers the vortex structure in the wake as freely deformable vortex grid and is therefore capable of simulating unsteady rotor motions with a high level of accuracy. The extreme platform pitch motions of the FOWT, where the rotor blades come close to the previously released vortices, can be modelled in much more detail by *pan*MARE than by BEMT methods. The influence of the wake on the blade forces can also be observed during a blade pitch action. Using a lifting line method, which also directly models the wake, Hauptmann [4] demonstrated the differences between BEMT and free wake methods investigating a pitching wind turbine blade. Roura [5] successfully validated a panel method similar to *pan*MARE against various measurements and therefore provided evidence for the applicability of panel methods for wind turbine rotors.

Widely used simulation programs like Hydrodyn, SIMO or Charm3D use coefficients matrices from potential flow based frequency domain analysis [6] (e.g. from WAMIT) to estimate the forces acting on the FOWT due to hydrostatics and hydrodynamics. Additionally, viscous effects can be included using simplified Morison elements. The other main group of hydrodynamic simulation programs (eg. BLADED and 3Dfloat) uses Morison-based formulations including several approximations to account for wave excitation forces, added mass, water surface elevation, and other effects. Both approaches are not capable of modelling the instantaneous flow field including the exact shape of the wetted surface area of the structure. However, both approaches show reasonable agreement with measurements under moderate conditions (eg. [7, 8]). *pan*MARE resolves a simplified three-dimensional flow field in order to compute the forces acting on the platform by integrating the pressure forces on the submerged part of the platform hull. In contrast to Morison or frequency analysis based methods, in the time domain simulation the buoyancy forces and moments are computed based on the instantaneous wetted surface area. This can lead to a considerable improvement of the simulation accuracy. In addition, this representation allows for considering more sophisticated phenomena in the future, such as the simulation of the unsteady deformation of the free water surface.

Combining different simulation methods such as BEMT and frequency analysis for aerodynamics and hydrodynamics with a six-degrees-of-freedom solver (6DOF) requires an implicit coupling procedure. As such, all solvers need to carry out the computation several times in each time step in order to obtain a converged solution. In virtue of the usage of a single potential flow solver for both aerodynamics and hydrodynamics, *pan*MARE computes aerodynamic, hydrodynamic, and mooring forces as well as the platform motion simultaneously using a fourth-order Runge-Kutta (RK4) time marching scheme. Therefore, an implicit iteration scheme is not needed, which leads to great savings in computational time.

By resolving the three-dimensional flow fields, *pan*MARE allows for a detailed analysis of FOWT dynamics beyond the common scope. Highly unsteady effects such as the dynamic behaviour of the platform during a fast change of the blade pitch or platform motions due to extreme waves as well as the performance of new FOWT concepts such as multi-rotor configurations or self-aligning platforms can be simulated in detail.

1.1 Scope of This Work

The Offshore Code Comparisons (OC3 [9] and OC4 [10]) have provided a large database for the verification of coupled simulation methods for FOWTs. Numerous implementations of different methods for aerodynamics, hydrodynamics, and mooring dynamics were coupled by the participants and their results were compared extensively. The dynamic behaviour of the NREL 5MW Reference Turbine [11] mounted on the DeepCWind Floater (see Figure 5) in several load cases is the subject of the OC4 Phase II simulations. In order to verify the developed simulation method *pan*MARE, a comparison of the OC4 Phase II data with our results, focussing on the hydrodynamic part, is carried out in this work. A fault load case containing a mooring line loss is slightly modified, resulting in even larger displacements. Having demonstrated the capability of the

simulation method to predict the dynamic behaviour of the FOWT, additional load cases containing a yaw motion of the turbine nacelle and wind-current misalignment will be analysed to determine the influence of dynamically varying aerodynamic loads on the floating condition.

2 METHODOLOGY

The three-dimensional flow fields around the rotor and the platform are modelled using the panel method *pan*MARE, which is based on potential flow theory. Initially, the method was developed to simulate the flow field of marine propellers [12]. In a further step, the capability of predicting the motion behaviour of floating and submerged bodies has been implemented and analysed in [13] and [14]. These preparatory works lead to excellent preconditions for a combined simulation of a turbine on a floating platform.

The flow fields of the rotor and the floating platform are treated in separate computational domains, but the solution procedures of both domains are carried out simultaneously using the same algorithm. This allows for an exchange of data between the fluid domains, the mooring model, and the 6DOF in every stage of the RK4 time marching scheme. A description of the individual models and their coupling is given in the following sections.

2.1 Panel Method

Assuming incompressible, irrotational, and inviscid flow a potential function Φ can be calculated whose gradient represents the velocity components. Applying these assumptions to the continuity equation in a closed domain and substituting the potential leads to Laplace's equation.

$$\Delta\Phi = 0 \tag{1}$$

Where the potential Φ combines an external potential Φ_{ext} (amongst others for inflow velocity), the body induced potential Φ_{ind} as well as the potential of the body's motion Φ_{motion}.

$$\Phi = \Phi_{ext} + \Phi_{ind} - \Phi_{motion} \tag{2}$$

Moreover, it can be shown that every velocity field obtained from a potential Φ under consideration satisfies the Navier-Stokes equations when applying the above-mentioned assumptions [15]. Hence, the velocity field in any domain can be obtained from a solution of Laplace's equation.

*pan*MARE obtains the flow field around a body by a superposition of the flow fields of source and dipole panels, which are surface distributed elementary solutions of Laplace's equation. Placing the source and dipole panels on the body's surface and postulating a Dirichlet boundary condition for the domain inside the body on their centre points prevents the flow from penetrating the surface. This leads to two conditions on every centre point for the source strengths σ_i and the strength μ_i.

$$-\frac{1}{4\pi}\int_{body\ panels}\sigma_i\frac{1}{r}dA + \frac{1}{4\pi}\int_{body\ panels}\mu_i\frac{\partial}{\partial\vec{n}}\left(\frac{1}{r}\right)dA = 0 \tag{3}$$

$$\sigma_i = \nabla(\Phi_{ext} - \Phi_{motion})\cdot\vec{n} \tag{4}$$

$\vec{n}$: panel normal, r: distance to centre point, dA: inf. surface element

The influence of the other source and doublet panels on the potential at the panel's centre point is represented by the sum terms. A detailed derivation of the introduced equations is given in [15]. Based on the potential, the velocity $\vec{v}$ and pressure p on the panel are calculated at its position $\vec{\theta}_p$.

$$\nabla\Phi = \vec{v} \tag{5}$$

$$\frac{p}{\rho} = \vec{g}\cdot\ \vec{\theta}_p - \frac{1}{2}(\nabla\Phi)^2 - \frac{\partial(\Phi)}{\partial t} \tag{6}$$

ρ: fluid density, $\vec{g}$: gravitational acceleration

Due to the assumption of inviscid flow, potential theory based methods do not account for skin friction, which may lead to an insufficient prediction of the drag force. To overcome this limitation, a Reynolds-dependent skin friction drag correction is implemented in *pan*MARE. The skin friction coefficient is calculated

based on the local Reynolds number, which is calculated at the centre of each panel along a streamline starting at its particular stagnation point. Utilising the "Schoenherr line", an additional force in line with the streamline is applied at the panel's centre. More details on the computation of the friction force is given in [16].

2.2 Aerodynamic Modelling

When considering a wing (or a rotor blade) additional dipole panels are placed in the wake in order to model the circulation shed from the trailing edge of the blade. The additional wake panels need be considered such that the Dirichlet boundary condition is satisfied. Thus, the second sum term in Eq. (3) is extended to consider the additional dipole panels of the wake.

As the wind turbine is subjected to unsteady inflow conditions due to the motion of the platform or fluctuation of the wind speed, the circulation on the rotor blades will change over time. Therefore, new wake panels are shed from the trailing edge of the rotor blades in every time step while older wake panels are moved with the local flow velocity. Applying the Kutta condition (7) at the trailing edge of a blade section ensures that the streamlines are aligned on the blade surface. The dipole strength of the newly emerging wake panels $\mu_{wake\,new}$ can then be expressed as a function of μ_{upper} and μ_{lower}, the strength of the upper and lower body panels at the trailing edge.

$$\mu_{wake\,new} = \mu_{upper} - \mu_{lower} \tag{7}$$

Due to the free wake alignment, a realistic distribution of the shed dipole panels and thus a realistic unsteady vortex structure can be achieved. When the length of the wake simulated increases, some wake panels may come close to each other and thus unphysical velocities and deformations can occur due to the singular character of the panels near their edges. To avoid this effect, the wake panels are transported with the local mean flow velocity when their location exceeds a certain distance to the rotor.

2.3 Hydrodynamic Modelling

The panel method *pan*MARE is also able to predict the hydrostatic and hydrodynamic forces on a floating or submerged body. The ability and function is described in [13] and [14] for the manoeuvring of ships in waves.

On the basis of the panel method described above, the velocity potential is solved. Furthermore, an acceleration potential is applied to calculate the unsteady flow field. It is defined as the substantial time derivative of the potential function Φ, see [17].

$$\frac{d\Phi}{dt} = \frac{\partial\Phi}{\partial t} + \vec{v}\cdot\nabla\Phi \tag{8}$$

Hence the Laplace equation of the acceleration potential yields:

$$\Delta\frac{d\Phi}{dt} = \nabla^2\frac{d\Phi}{dt} = 0 \tag{9}$$

Solving the acceleration potential demands some additional computational effort at each iteration but provides more details of the flow field with higher accuracy, which improves the quality of the calculated dynamic pressure and the stability of the computation. Based on the acceleration potential, an advanced method of added mass matrix calculation is used, which is described in [18]. The method only enlarges the right-hand side of the equation system, without influencing the coefficients and thus leads to a slight increase of the computational effort only.

Immersion of Panels

Depending on the platform position and wave elevation, the immersion of panels changes over time. A split technique is used to estimate the immersion of each particular panel at each iteration. If all corners of a panel are immersed, the split factor of the panel will be set to one, and otherwise to zero, for totally emerged panels. The split factor of partly wetted panels is given with the immersion of panel corners p_i, where d_i is the depth of the corner measured from the actual surface location, referring to Figure 1.

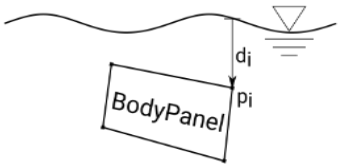

Figure 1: Split factor calculation

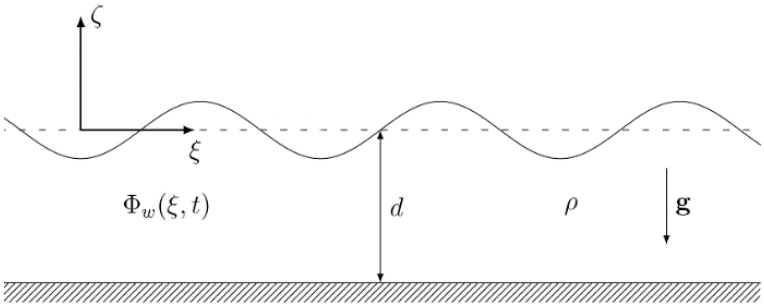

Figure 2: Wave definition

$$S_P = \begin{cases} 1 & \min(d_i) \geq 0 \\ \dfrac{\max(d_i)}{\max(d_i) - \min(d_i)} & \min(d_i) < 0 < \max(d_i) \\ 0 & \max(d_i) \leq 0 \end{cases} \tag{10}$$

Emerged panels are deactivated and the influence of partly immersed panels is reduced to represent the grade of immersion. The immersion depth depends on the actual floating condition of the platform and the wave elevation at the corner points. In this way, the instantaneous platform position and wave elevation is considered when solving the fluid and calculating the pressure on the immersed hull. The emerged hull of the floating substructure is not part of the hydrodynamic modelling and as it has limited influence on the aerodynamic loads, its contribution is neglected in the aerodynamic solution.

Waves

For the description of regular waves and the seaway the linear wave theory is applied. With the characterising parameters (see Figure 2) of amplitude ζ_a, wave angular frequency ω, wave number k, and water depth d, the potential is given for a particular position in Cartesian coordinates $\vec{\theta} = [\xi, \eta, \zeta]^T$ at an instant of time t:

$$\Phi_w(\vec{\theta}, t) = -\zeta_a \frac{\omega}{k} \frac{\cosh\big(k\,(\zeta - d)\big)}{\sinh(k\,d)} \mathrm{Re}\big\{i\, e^{i\,(-\omega t + k\,\bar{\xi} + \epsilon)}\big\} \tag{11}$$

Where $\bar{\xi}$ describes the horizontal distance from any point in the field to the wave reference point along the wave propagation direction and ϵ the wave phase shift. The seaway is represented using an array of linear waves. Individual waves can have different directions to reproduce two-dimensional seaway conditions. Φ_w is considered in the computation as an external potential.

Morison Elements

As viscous drag effects are neglected in the velocity potential, their contribution to the pressure resistance cannot be considered in the flow field. To overcome this drawback of the potential theory, cylindrical Morison elements are introduced for the body parts not included in the fluid solution. The resulting forces are based on the total fluid velocity on the elements' centre, including their motion velocity and acceleration. Buoyancy forces are considered as well. In the simulation, Morison elements are used to represent slender bodies, which have little influence on the flow field.

Forces of a Morison element depending on water density ρ, body diameter D, length l, and gravitation $\vec{g}$ are calculated using the following equation.

$$\vec{F}_M = \underbrace{\rho \frac{\pi D^2}{4} l \frac{\partial \vec{u}_N}{\partial t}}_{Froude-Krylov} + \underbrace{C_a \rho \frac{\pi D^2}{4} l \frac{\partial \vec{u}_{RN}}{\partial t}}_{Added\ Mass} + \underbrace{C_d \frac{\rho}{2} D l \vec{u}_{RN} |\vec{u}_{RN}|}_{Drag} - \underbrace{\rho \frac{\pi D^2}{4} l \vec{g}}_{Buoyancy} \tag{12}$$

The relative flow velocity $\vec{u}_R$ is the sum of induced and external velocities at the element's centre. The absolute flow velocity is $\vec{u}$. Subscript $_N$ denotes the orthogonal velocity using the panel normal.

Morison Drag Elements

To consider the form drag forces of panelled bodies, which are part of the fluid solution, a reduced Morison element is implemented. It is a reduction of equation (12) to the drag term. Moreover, the relative flow velocity only implies the external and motion velocity on the element's centre. The induced velocity is excluded to match the definition of the drag coefficient, which does not imply the influence of the body on the velocity.

Overall, the hydrodynamic modelling with panels and Morison elements captures Froude-Krylov, added mass, drag, and hydrostatic forces using the instantaneous wetted hull surface area.

2.4 Mooring

A mooring line system is essential to keep the platform in position, while waves, current and wind loads act in arbitrary directions. As the mooring system compensates the rotor thrust and damps platform motions, its influence on the platform's motion behaviour is significant.

A quasi-static mooring model is implemented, which has been derived in [19]. The formulation assumes a homogenous line with constant diameter, weight, and Young's modulus and gives the shape and forces of a hanging line touching the ground. Due to the quasi-static approach, inertia forces are not considered. Additional fluid forces from current or waves are neglected and do not have an influence on the shape of the line or line end forces. Hence the forces on the fairlead and anchor point depend on the fairlead position only.

This method is rather simple but allows a fast and robust calculation of the fairlead forces. The integration into the coupling and time marching procedure is straight forward, since none of the considered values is time dependent.

2.5 Coupling and Time Marching

The main aim of such detailed simulations of aerodynamics, hydrodynamics, and the mooring system is to improve the accuracy of the predicted motion. Maximum accelerations and angular deflections exert a major influence on design loads and therefore a sufficiently resolved time marching is inevitable.

The Newton-Euler equations describe the motion of a rigid body in six degrees of freedom (6DOF) in a Cartesian coordinate system, see Figure 3.

$$\boldsymbol{M}\frac{d^2\vec{r}}{dt^2} = \vec{q}\left(\vec{r}, \frac{d\vec{r}}{dt}, \frac{d^2\vec{r}}{dt^2}, t\right) \tag{13}$$

The combined mass and inertia matrix

$$\boldsymbol{M} = \begin{bmatrix} m_{Body}\boldsymbol{I}_{3\times3} & \boldsymbol{0}_{3\times3} \\ \boldsymbol{0}_{3\times3} & \boldsymbol{J}_{Body} \end{bmatrix} + \boldsymbol{M}_{Added\ Mass} \tag{14}$$

resulting from the mass m_{Body} and inertia tensor $\boldsymbol{J}_{Body}$ of the body and identity matrix $\boldsymbol{I}$ and zero matrix $\boldsymbol{0}$, respectively. The position of the centre of gravity and the orientation of the body is described in generalised coordinates. The angles denote intrinsic Euler angles with platform roll angle φ, platform pitch angle γ and platform yaw angle ψ.

$$\vec{r} = [\xi, \eta, \zeta, \varphi, \gamma, \psi]^T \tag{15}$$

The combined forces and moments $\vec{q}$ are dependent on position, velocity, and acceleration of the body as well as time. The right-hand side of equation (13) is the sum of all forces and moments plus gyroscopic moments and additional added mass forces and moments.

$$\vec{q} = \boldsymbol{M}_{Added\ Mass} \cdot \frac{d^2\vec{r}}{dt^2} - \begin{pmatrix} [0,0,0]^T \\ \vec{\omega} \times (\boldsymbol{J} \cdot \vec{\omega}) \end{pmatrix} + \sum q_i' \qquad \text{with } \vec{\omega} = [\dot{\varphi}, \dot{\gamma}, \dot{\psi}]^T \tag{16}$$

The sum of q_i' contains all fluid and mooring force-moments and gyroscopic moments induced by the rotor rotation.

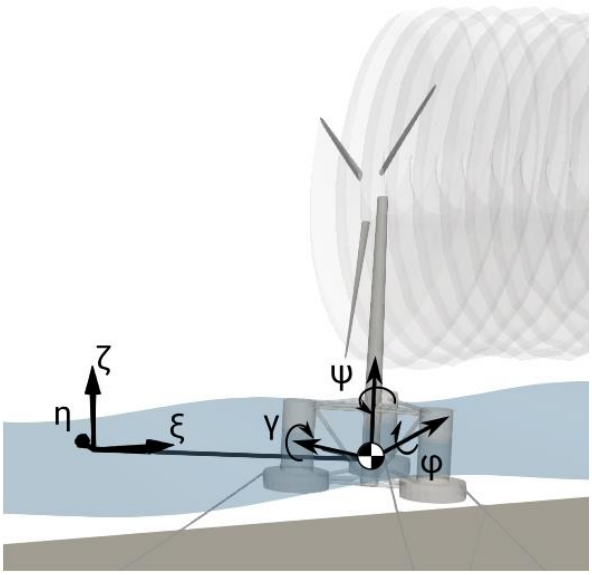

Figure 3: General coordinate system

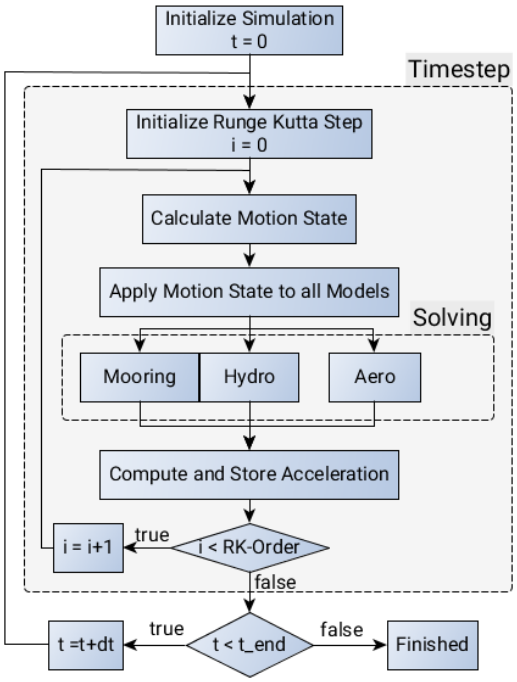

Figure 4: Flowchart of the fully integrated solving procedure using an explicit Runge-Kutta method

Solving equation (13) yields translational and rotational accelerations. Integration is necessary to obtain the velocities and finally the translation and rotation. Different Runge-Kutta integration schemes are implemented in *pan*MARE's motion solver. Explicit and implicit Euler methods allow for a straight forward time marching by iterating implicitly to a converged solution at every time step.

A more sophisticated integration can be achieved by using higher-order Runge-Kutta methods. Higher accuracy and/or larger time steps are possible and lead to higher efficiency. However, within one time step, coupled simulation models for the aero- and hydrodynamic parts as well as the mooring system must perform the same motions at each iteration. Thus, they need to be coupled closely. Using the same solver for aero- and hydrodynamic domains makes this rather simple. The mooring model depends on the hydrodynamic geometry model and thus fits into the iteration loop. The time step iteration scheme is shown in detail in Figure 4.

Wave elevation and wave potential are updated at each iteration and the rotor's wake deformation performs every stage of the iteration scheme explicitly.

3 MODEL SETUP

To investigate *pan*MARE's capability of simulating a FOWT, a comparison with the extensive Offshore Code Comparison Collaboration Continuation (OC4) project is carried out. Various institutes have modelled the semisubmersible platform equipped with the well-known NREL5MW reference turbine. The platform consists of three main columns with a massive heave plate on each bottom and one centre column. Several cross braces connect the four columns. The turbine is placed on a nearly 90m tower on the centre column and three mooring lines keep the platform in position. Detailed dimensions and setup information can be found in [11] and [20].

An overview of the model's components is given in Figure 5. Platform, tower, and rotor are considered as rigid bodies. The rotor can rotate freely using a one-dimensional motion solver with counter torque from the generator and a simple PID blade pitch controller. Body panels and additional Morison drag elements are used to model the main and centre columns of the platform, which represent the bigger parts. The smaller elements, cross-braces between the columns, are modelled with Morison elements. A detailed view on the platform is given in Figure 6. It also shows the split factors of the panels.

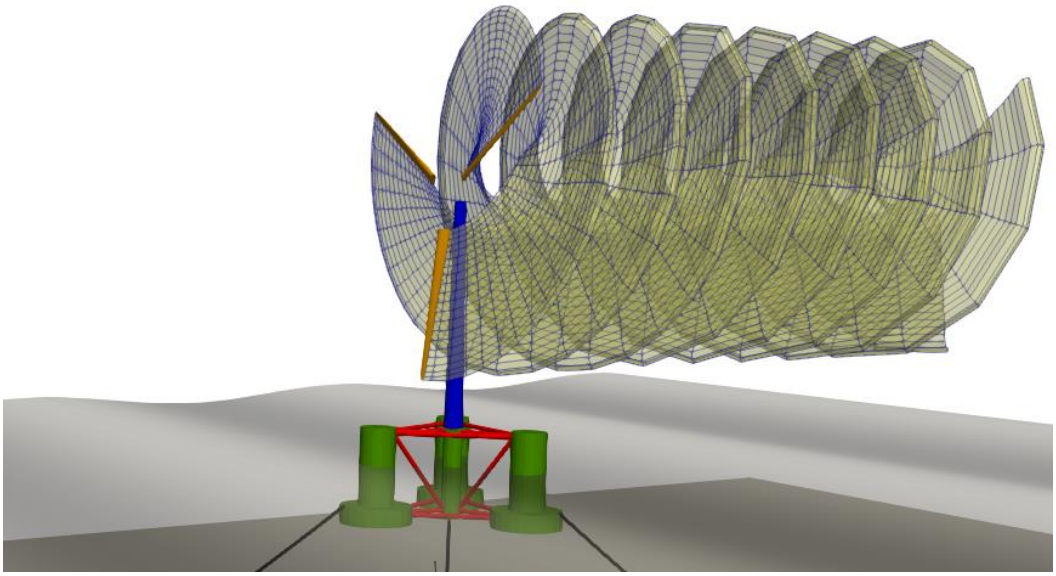

Figure 5: Model setup with platform (green: body panels and Morison drag elements, red: Morison elements), tower (blue), rotor blades (orange), rotor wake (yellow), mooring, and water surface

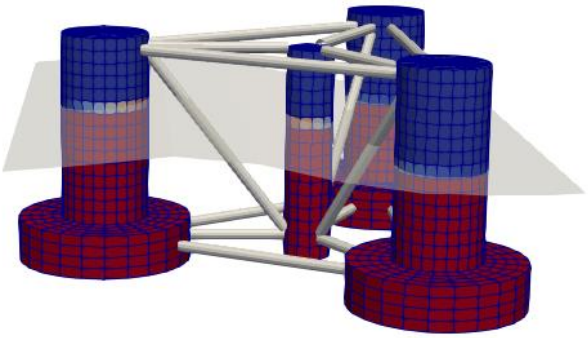

Figure 6: Platform body panels coloured by their split factor (red: 1.0, blue: 0.0)

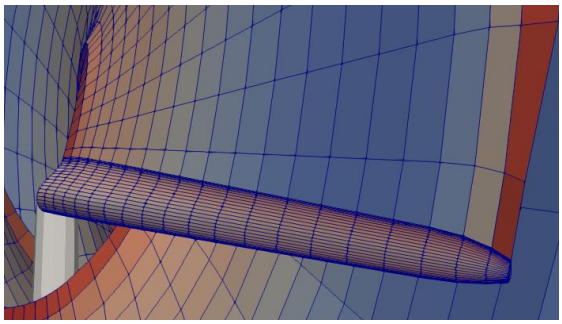

Figure 7: Grid of a rotor blade and the corresponding wake panels with dipole strength

Tower and rotor on the aerodynamic side are discretized with body panels as well. To prevent extreme induced velocities due to singularities at panel edges when rotor wake and tower cross, the influence between tower and wake is limited. For the sake of simplicity, nacelle and hub are neglected. The cylindrical part at the root of the rotor blades has been omitted to avoid the inaccuracies induced by the stall regions. The length of the wake has a major influence on the rotor thrust and torque. Thus, a length of nearly two times the rotor diameter is considered in the simulation, which leads to different numbers of panels at different wind speeds. The rotor grid and the beginning of the wake are shown in Figure 7.

The number of panels and Morison elements used in the simulation is given in Table 1. Nearly 10,000 panels are used for an inflow velocity of 8m/s where the half is applied on the wake to achieve the required wake length.

Table 1: Discretization details

Domain	**Part**	**Elements**
Hydrodynamic	Platform	2496 Body Panels
	Platform (Morison)	139 Elements
Aerodynamic	Tower	144 Body Panels
	Rotor	3150 Body Panels
	Wake at 8 / 18 m/s	5760 / 3000 Wake Panels

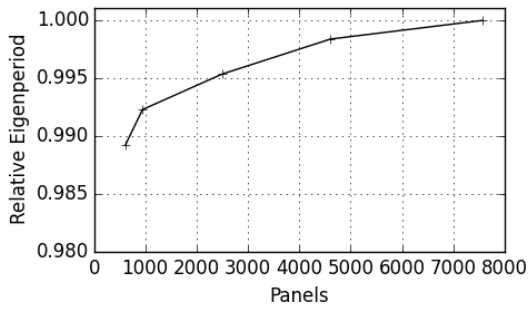

Figure 8: Platform grid refinement

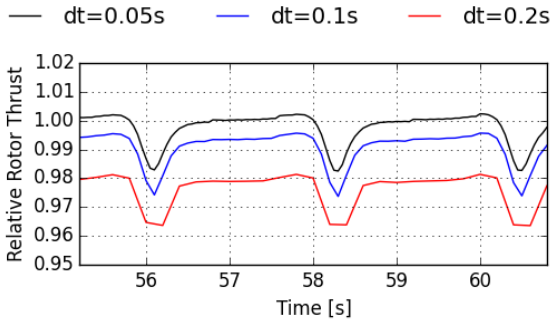

Figure 9: Unsteady relative rotor thrust

The influence of the discretization of the platform on the calculated results is investigated. Free decay simulations with heave excitation have been conducted for different numbers of panels. The same setup was used here as used for load case 1.3b (see the verification section below). As shown in Figure 8, the grid refinement has a slight influence on the calculated natural frequency of heave motion. A discretization with nearly 2500 body panels was found to give sufficient results, with an error of below 0.5 percent compared to an extremely fine discretization.

The time step size is mainly influenced by the aerodynamic simulation. When a blade passes in front of the tower, a peak on the rotor forces occurs. A time step of 0.1 seconds has been chosen to clearly capture this peak, see Figure 9.

4 VERIFICATION

Various load cases have been defined in the OC4 project and a large number of participants provided the results of different simulation codes. Subsequently, the load case definitions and results are presented and analysed in [10]. All results and further load case information are published and available also online.[1]

To evaluate the capabilities of the presented method, the results of *pan*MARE for a selection of load cases (Table 2) are presented below and compared with a selection of the OC4 participants. The first set of simulations (1.3a to 1.3b) is carried out to identify the most important characteristics influencing the dynamic of the floating system. They are reduced to the hydrodynamic simulation and mooring model in still water. Aerodynamic influences are neglected. The same holds true for the second set, where waves are added to excite the platform (only load case 2.1 is shown here). The third set of load cases involves the aerodynamic model and a small representation of operation and fault conditions. A modified mooring line loss load case 3.8* is added, where the front mooring line is lost.

The selection of the first set consists of four free decay tests with enforced excitations regarding surge, heave, pitch, and yaw motion. In general, a good agreement with the presented data in OC4 can be observed for all load cases (Figure 10 to Figure 13). Only in surge and yaw motion a small deviation of the decay period is noticeable. In all other cases the results of *pan*MARE are almost identical to most OC4 participants. The large discrepancies of some OC4 participants may be due to a different drag modelling.

Table 2: Load cases

Load case	Name	Description
1.3a	Free decay, surge	Initial surge = +22m, no aerodynamics
1.3b	Free decay, heave	Initial heave = +6m, no aerodynamics
1.3c	Free decay, pitch	Initial pitch = +8°, no aerodynamics
1.3d	Free decay, yaw	Initial yaw = +8°, no aerodynamics
2.1	Regular wave	Linear wave (H=6m, T=10s), no aerodynamics
3.1	Wind and regular wave	Linear wave, steady wind (8m/s)
3.4	Wind-wave-current	Linear wave, steady wind, and current (0.5m/s)
3.6	Wind-wave misalignment	Misalignment of 30°
3.8	Mooring line loss	Loss of sideward mooring line with steady wind (18m/s)
3.8*	Front mooring line loss	Loss of front mooring line with steady wind (18m/s)

[1] https://drive.google.com/drive/folders/0B0KGNSHvXXgCSDBlREZLdDRxX2s

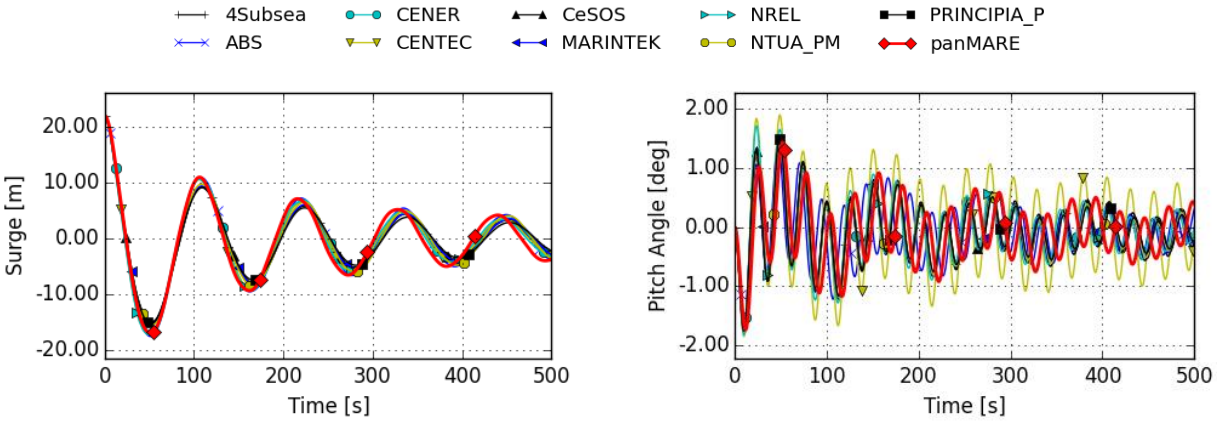

Figure 10: LC1.3a, free decay, initial surge +22m

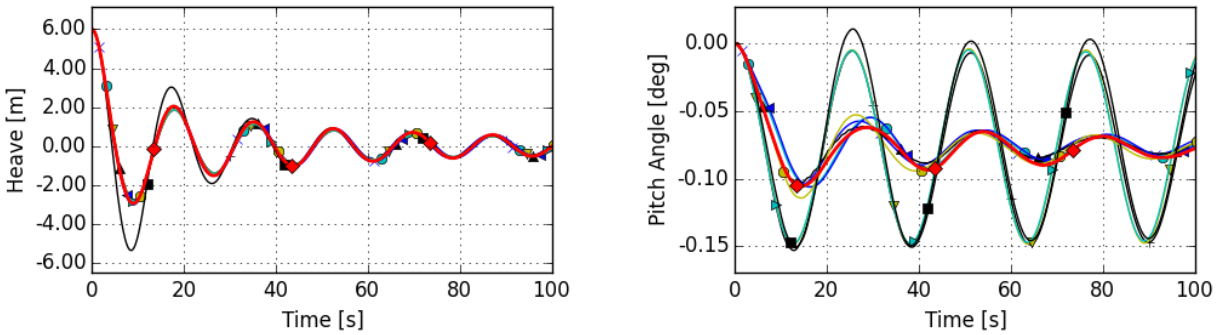

Figure 11: LC1.3b, free decay, initial heave +6m

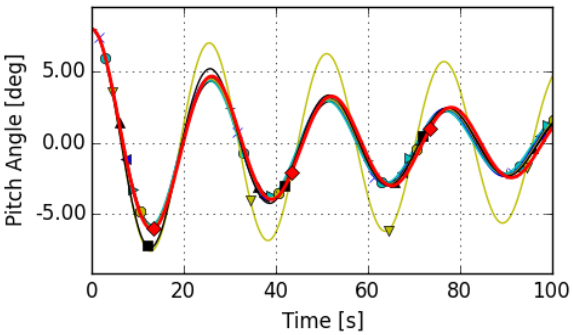

Figure 12: LC1.3c, free decay, initial pitch +8°

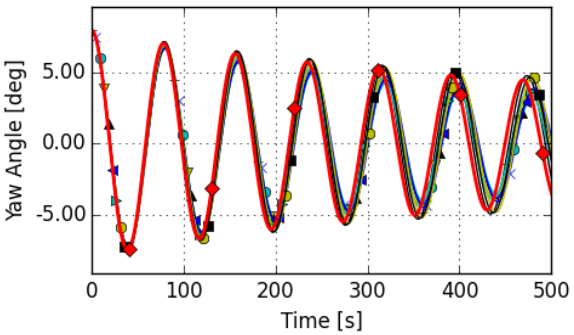

Figure 13: LC1.3d, free decay, initial yaw +8°

The same setup is applied on load case 2.1, where, in this case, the excitation is induced by regular waves, see Figure 14. Heave and pitch meet the referencing results very well. Load case 3.1 has the same hydrodynamic conditions but the aerodynamic model is activated and the turbine is operating under partial load condition. The results again show good agreement, see Figure 15. The turbine's thrust reduces the heave motion and leads to a positive mean pitch angle of the platform.

In load case 3.4, current is added to the wind and waves. Figure 16 and Figure 17 show the influence of the current on the platform's surge. With no current *pan*MARE overestimates the influence on the mean surge displacement slightly, but matches the amplitude. While under consideration of the acting current speed, the results of the OC4 participants differ in their mean value and the predicted surge of *pan*MARE is within the upper range. In this case, the mean value is different too, but the motion amplitude predicted shows good agreement with other results presented in OC4.

Wind-current misalignment leads to a sway and roll motion of the platform, shown in the results of load case 3.6 in Figure 18. The predicted sway motion of selected OC4 participants and *pan*MARE differ in their mean value but show similar amplitudes. A good agreement is achieved on the platform roll motion.

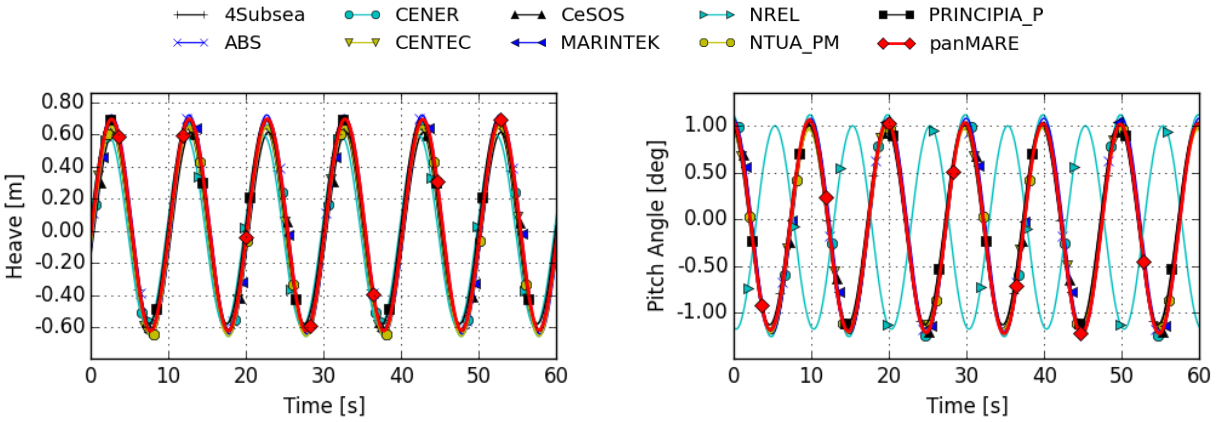

Figure 14: LC2.1, regular waves

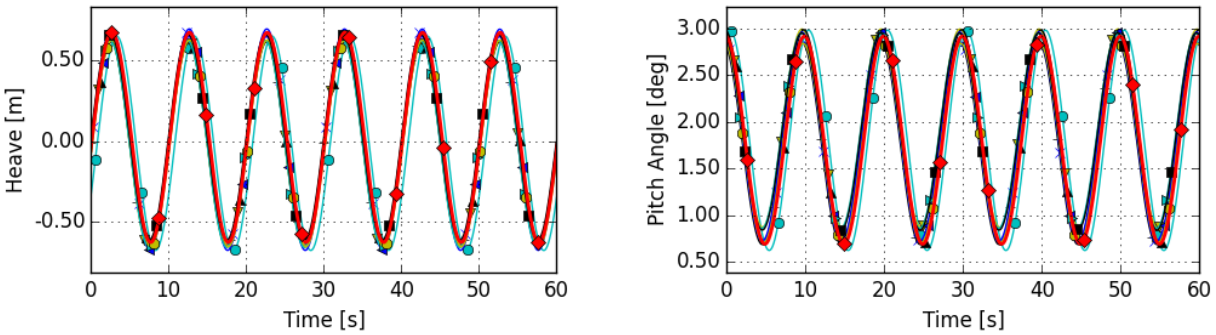

Figure 15: LC3.1, regular waves with operating turbine

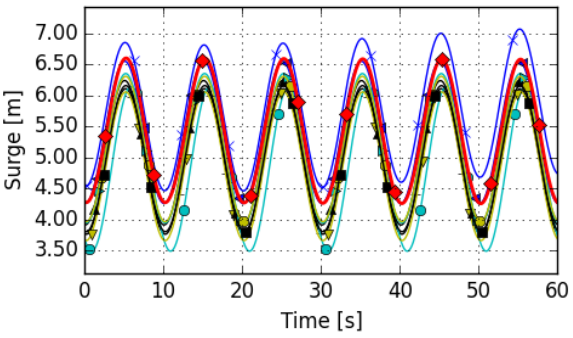

Figure 16: LC3.1, surge motion

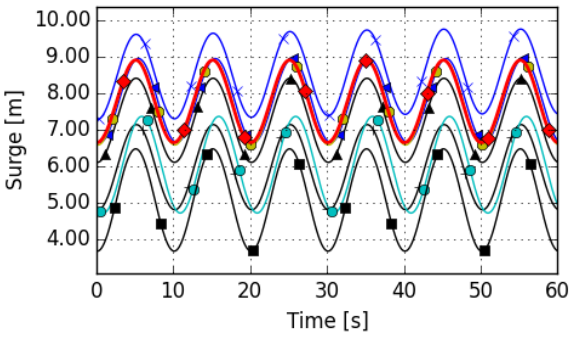

Figure 17: LC3.4, wind, waves and current

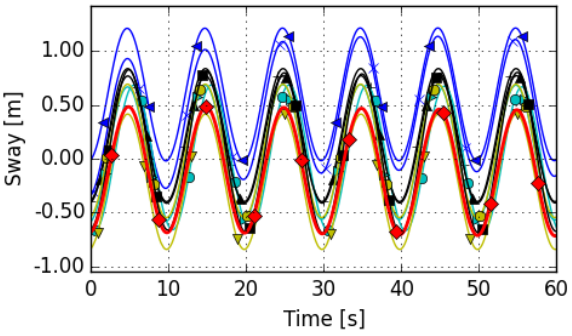

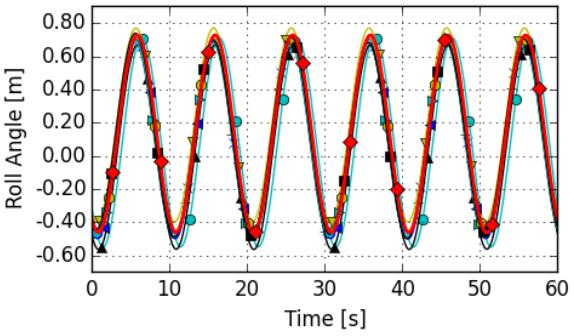

Figure 18: LC3.6, wind-wave misalignment

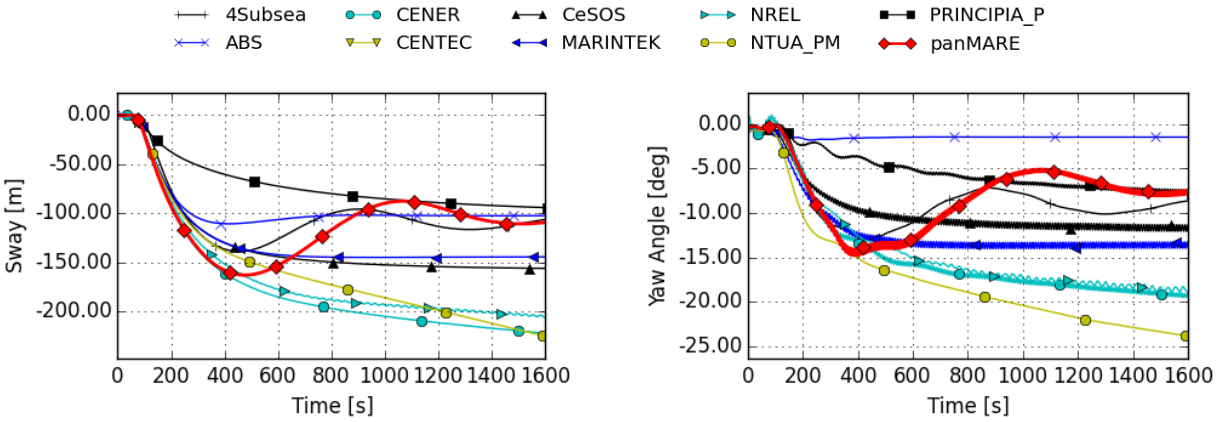

Figure 19: LC3.8, mooring line loss

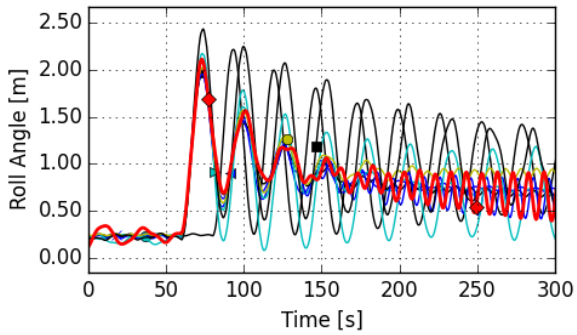

Figure 20: LC3.8, mooring line loss details

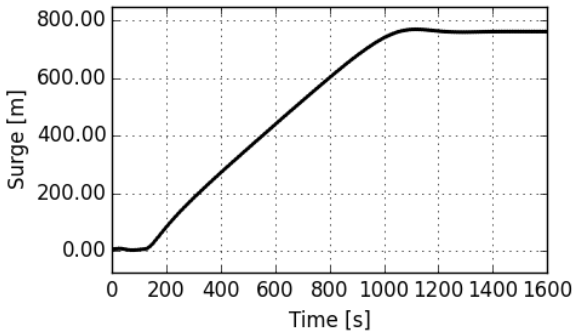

Figure 21: LC3.8*, front mooring line loss

Load case 3.8 considers the loss of mooring line 1, which is connected to the left column in the back in the direction of wind and wave. The line fails 60 seconds after the beginning of the plot. The calculated sway displacement and the platform yaw angle can be seen in Figure 19. Both quantities show varying values after nearly half an hour of simulation time, which can be considered as the steady state (apart from the waves) for some methods whereas the results of others still show platform sway motion up to 200m. As the steady state in sway and yaw is determined by a balance of rotor and mooring loads in nearly steady conditions, the reason for the occurrence of these differences could not be identified. Considering the mooring models, it is shown in [10] that the tension of the mooring lines in regular waves does not show significant deviations between the OC4 participants. As most simulation tools utilise the same underlying theory, it is not likely that significant differences in aerodynamic loading cause the deviations.

In *pan*MARE, a yaw controller is used causing the yaw actuator to turn the nacelle +10° at 363 seconds. In this case, the response including an overshoot is clearly visible. A similar behaviour can be observed in the 4Subsea results. As a yaw controller was not defined for the OC4 simulations, the deviations between *pan*MARE and other participants may be due to differences in yaw control.

Looking at the response of the roll angle to the mooring line loss in Figure 20, it can be observed that some participants predict a low damping whereas the roll motion obtained by *pan*MARE agrees well with most other participants' results.

The results of this load case show that the simulation remains stable even at large displacements. As one mooring line remains under tension during the simulation, the motion is still guided. A variation of this load case has been constructed under the number LC3.8*. Losing the connection to the mooring line 2 at the front column leads to a relaxation of mooring lines 1 and 3 and therefore allows for an almost free drift of the platform until the mooring lines are subjected to tension again. Figure 21 illustrates the surge motion of the platform, showing such an expected behaviour. This demonstrates that even large displacements and free drift motions do not lead to instability issues in *pan*MARE.

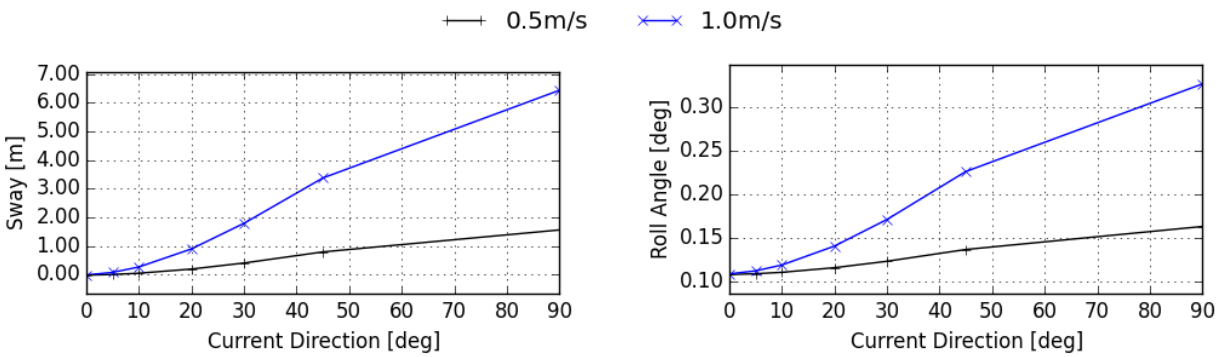

Figure 22: Steady state sway and roll over misalignment angle for 0.5m/s and 1.0m/s current velocity

5 WIND-CURRENT MISALIGNMENT

Wind and current misalignment is a very likely event at most potential locations of FOWT. The prediction of the platform orientation under such conditions is a major advantage of *pan*MARE, since there are little restrictions on large deformations.

The steady state orientation of the platform under various wind-current misalignment angles has been simulated under partial load. The turbine operation conditions equal load case 3.1, with a wind velocity of 8m/s and a rotor rotational speed of 9PRM. No waves are acting to reduce overlaying effects. Current velocity of 0.5 m/s and 1.0 m/s are applied with a power law exponent of 1/7. The steady state sway and roll angles are shown over the misalignment angle in Figure 22. The increasing sway displacement is evident but the side current also effects the roll angle of the platform. As the drag force on the platform is dependent on the square of the current velocity, it is reasonable that the displacement grows more than linear with the current velocity.

6 YAW DYNAMICS

The dynamic response of a FOWT during a yaw alignment of the rotor is highly dependent on the mooring system. A slack mooring leads to an overshoot of the platform yaw motion due to inertia effects and might even cause a gain of small rotor yaw misalignments when the yaw actuator is inactive. The mooring of the studied FOWT is designed tautly such that the dynamic response is relatively small but still the principal effects can be observed.

Figure 23 shows the response of the platform yaw angle to a rotor yaw event. Beginning with axial inflow, the wind turns until the yaw misalignment reaches 15° at 300 seconds of simulation. Ten seconds later the yaw drive rotates the nacelle with a speed of 0.3°/s until the yaw misalignment reaches zero at 360s. With the onset of the rotor yaw activity, the response of the platform yaw angle rises due to inertia effects and a change of the rotor yaw moment. A more interesting phenomenon can be observed in the platform surge motion, which shows a significant change just after the onset of the rotor yaw activity. Due to the platform inertia, the displacement reaches its maximum a few seconds after the yaw activity stops. As the rotor thrust acts in line with the rotor axis, the yaw misalignment occurring at 240s has negligible influence on the platform surge. Therefore, at moderate yaw angles, the activity of the yaw actuator itself determines the sway response. Thus, the overshoot in surge can be controlled by the yaw rate, which might be a useful fact for the development of FOWT yaw controllers.

7 CONCLUSION AND FUTURE WORK

In the presented paper, the panel method *pan*MARE is introduced as a simulation tool for FOWTs. The simulation results show that compared to similar coupled methods *pan*MARE has the ability to model the three-dimensional unsteady aerodynamic and hydrodynamic flow fields. Therefore the obtained results include a more detailed representation of the underlying physics. Focussing on the hydrodynamic effects, the dynamic behaviour of the OC4 Phase II semisubmersible FOWT is predicted for several load cases and compared to the results from the OC4 participants. Additional load cases are constructed in order to investigate *pan*MARE's capability to account for the dynamics due to yaw controller activities, wind current misalignment, and large displacements.

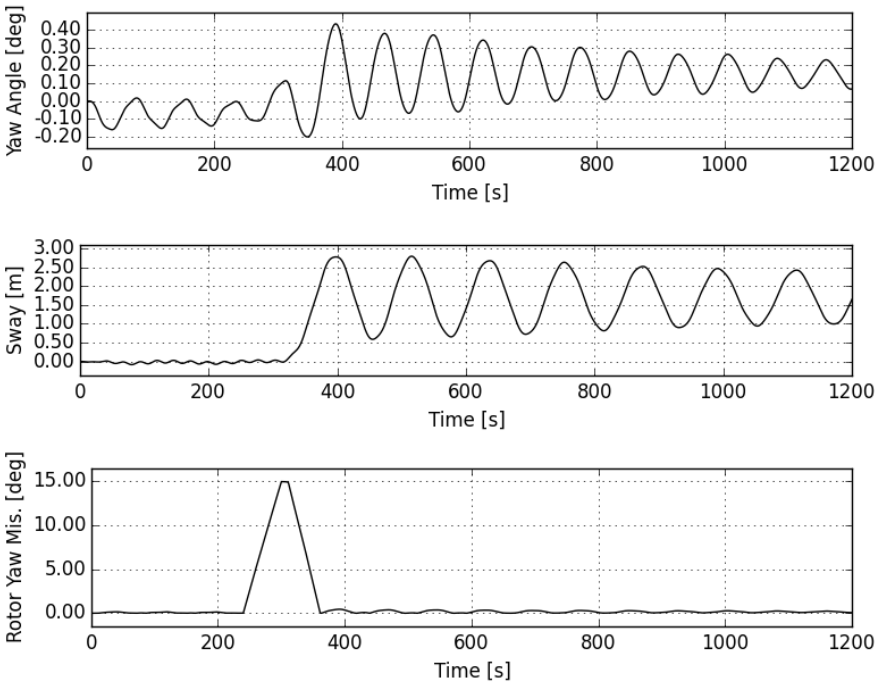

Figure 23: Dynamic yaw misalignment, yaw angle, sway motion and rotor yaw misalignment

The verification against the OC4 results shows good agreement for all considered load cases apart from the mooring line loss scenario, where the predicted trajectories diverge strongly between the participants. Considering the free decay tests very similar results can be observed for nearly all participants and *pan*MARE. Unfortunately, the extreme wave scenario is difficult to evaluate as the simulation time is too short to obtain statistically comparable input quantities from the JONSWAP spectrum. Coupled wind-wave simulations including current at the water surface can be conducted in a stable manner and compare well. The variations observed in the mooring line loss scenario might be caused by the usage of different yaw controllers. Nevertheless, in the period just after the loss of the mooring line *pan*MARE and most OC4 participants predict a similar trajectory of the FOWT. Differences occur when looking at the roll damping, which is predicted differently by the participants, whereas the damping obtained by *pan*MARE is similar to the majority of the results.

In combination with the additional load cases, it is shown in this work that the general dynamic behaviour of the FOWT can be predicted even in unsteady situations including large displacements. Capturing the influence of dynamically changing yaw misalignments and wind-current misalignment, *pan*MARE also allows for the examination of self-aligning FOWTs.

As the OC4 Phase II load cases do not contain directly comparable trajectories and motions of the FOWT in extreme or highly unsteady scenarios further validation is needed in order to quantify *pan*MARE's capabilities. Therefore, future work will focus on a more detailed validation of both the aerodynamic and the hydrodynamic part using experimental data. A further improvement of the mooring model using a dynamic lumped mass approach is planned. Utilising the advantages of the three-dimensional flow field, a free surface shall be implemented to capture the influence of radiation directly. When applying these high-fidelity models, *pan*MARE might close the gap between computationally extremely expensive CFD couplings and state-of-the-art design tools for FOWT dynamics.

ACKNOWLEDGEMENTS

The authors kindly thank the Federal Ministry for Economic Affairs and Energy of Germany (BMWi) for financially supporting the HySToH project (03SX409A-F) and our partners LINNHOFF Offshore AG, aerodyn engineering gmbh, JÖRSS – BLUNCK – ORDEMANN GmbH, DNV-GL and the Institute for Ship Structural Design and Analysis at the Hamburg University of Technology for the excellent cooperation.

REFERENCES

1 M. O. L. Hansen, J. N. Sørensen, S. Voutsinas, N. Sørensen, and H. A. Madsen, "State of the art in wind turbine aerodynamics and aeroelasticity", Progress in Aerospace Sciences, vol.42, no. 4, pp. 285–330, 2006.

2 D. J. Laino, A. C. Hansen, and J. E. Minnema, "Validation of the AeroDyn subroutines using NREL unsteady aerodynamics experiment data", Wind Energy, vol. 5, no. 2–3, pp. 227–244, 2002.

3 T. T. Tran and D. H. Kim, "The platform pitching motion of floating offshore wind turbine: A preliminary unsteady aerodynamic analysis", Journal of Wind Engineering & Industrial Aerodynamics, vol. 142, pp. 65–81, 2015.

4 S. Hauptmann , M. Bülk, L. Schön, S. Erbslöh, K. Boorsma, F. Grasso, M. Kühn, P. W. Cheng, "Comparison of the lifting-line free vortex wake method and the blade-element-momentum theory regarding the simulated loads of multi-MW wind turbines," J. Phys. Conf. Ser., vol. 555, no. 1, p. 12050, 2014.

5 M. Roura, A. Cuerva, A. Sanz-Andres, and A. Barrero-Gil, "A panel method free-wake code for aeroelastic rotor predictions," Wind Energy, vol. 13, no. 4, pp. 357–371, 2010.

6 A. Cordle and J. Jonkman, "State of the Art in Floating Wind Turbine Design Tools", International Offshore and Polar Engineering Conference, 2011.

7 A. J. Coulling, A. J. Goupee, A. N. Robertson, J. M. Jonkman, and H. J. Dagher, "Validation of a FAST semi-submersible floating wind turbine numerical model with DeepCwind test data", Journal of Renewable and Sustainable Energy, vol. 5, no. 2, p. 23116, 2013.

8 A. Myhr and T. A. Nygaard, "Comparison of Experimental Results and Computations for Tension-Leg-Buoy Offshore Wind Turbines", Journal of Ocean and Wind Energy, vol. 2, no. 1, pp. 12–20, 2015.

9 J. Jonkman and W. Musial, "Offshore Code Comparison Collaboration (OC3) for IEA Task 23 Offshore Wind Technology and Deployment", 2010.

10 A. Robertson, J. Jonkman, F. Vorpahl, J. Qvist, X. Chen, J. Azcona, E. Uzunoglu, C. G. Soares, C. Luan, F. Pengcheng, A. Yde, T. Larsen, R. Buils, L. Lei, T. A. Nygard, A. Heege, S. R. Vatne, T. Duarte, C. Godreau, H. Fabricius, A. W. Nielsen, H. Riber, C. Le, R. Abele, F. Beyer, A. Yamaguchi, K. Jin, H. Shin, W. Shi, H. Park, and M. Alves, "Offshore Code Comparison Collaboration Continuation Within IEA Wind Task 30: Phase II Results Regarding a Floating Semisubmersible Wind System", 33rd International Conference on Ocean, Offshore and Arctic Engineering, 2014.

11 J. M. Jonkman, S. Butterfield, W. Musial, and G. Scott, "Definition of a 5-MW Reference Wind Turbine for Offshore System Development", NREL Technical Report, 2009.

12 M. Bauer, M. Abdel-Maksoud, A 3-D Potential Based Boundary Element Method for the Modelling and Simulation of Marine Propeller Flows, 7th Vienna Conference on Mathematical Modelling, Austria, 2012

13 J. Schoop-Zipfel, M. Abdel-Maksoud, Maneuvering in Waves Based on Potential Theory, 33rd International Conference on Ocean, Offshore and Arctic Engineering (OMAE2014), 2014

14 D. Ferreira González, S. Loebus, and M. Abdel-Maksoud, "Application of a boundary element method for hydrodynamic simulations of landing manoeuvres at an offshore foundation," in International Workshop on Ship and Marine Hydrodynamics, 2015, no. August, pp. 26–28.

15 J. Katz and A. Plotkin. Low-Speed Aerodynamics. Cambridge University Press, Cambridge, second edition, 2001.

16 S. F. Hoerner. "Fluid-dynamic drag: practical information on aerodynamic drag and hydrodynamic resistance", Chapter 2.4, Skin-friction drag with turbulent boundary layer, Hoerner Fluid Dynamics, 1965

17 W. Johnson, "Rotorcraft Aeromechanics", Cambridge Aerospace Series, Number 36, Cambridge University Press, 2013.

18 W. Sichermann, "Zur Simulation und Vorhersage extremer Schiffsbewegungen im natürlichen Seegang", Thesis, Hamburg University of Technology, 2008.

19 M. Masciola, "MAP ++ Documentation", Release 1.15, 2017.

20 A. Robertson, J. Jonkman, and M. Masciola, "Definition of the Semisubmersible Floating System for Phase II of OC4", NREL Technical Report, 2014.